Magazine of Concrete Research
Volume 69 Issue 20

Wet swelling effect on crack performance of facing concrete for rockfill dams
Xu, Li, Hu and Li

Magazine of Concrete Research, 2017, **69**(20), 1055–1066
http://dx.doi.org/10.1680/jmacr.16.00367
Paper 1600367
Received 26/08/2016; revised 13/03/2017; accepted 27/03/2017
Published online ahead of print 25/05/2017
Keywords: cracks & cracking/strain/testing, structural elements

ice
Institution of Civil Engineers
publishing

Wet swelling effect on crack performance of facing concrete for rockfill dams

Wenbin Xu
PhD student, Department of Hydraulic Engineering, Tsinghua University, Beijing, China

Qingbin Li
Professor, Department of Hydraulic Engineering, Tsinghua University, Beijing, China

Yu Hu
Associate Professor, Department of Hydraulic Engineering, Tsinghua University, Beijing, China (corresponding author: yu-hu@tsinghua.edu.cn)

Shuguang Li
Senior engineer, State Key Laboratory of Simulation and Regulation of Water Cycles in River Basins, China Institute of Water Resources and Hydropower Research (IWHR), Beijing, China

The swelling of aged concrete is a significant issue in the operation of dams such as concrete-faced rockfill dams (CFRDs). Swelling of concrete is one cause of tensile stress, which is typically related to water movement in concrete pores, especially around the water surface. In this study, the change in the interior relative humidity and deformation in aged concrete specimens around the surface of the water were measured. The experimental results revealed that the swelling of the concrete above the water surface was correlated with an increase in interior relative humidity due to water diffusion, while the swelling of the concrete submerged in the water developed in early and late stages and was dominated by capillary absorption and diffusion. A new theoretical swelling model was developed to predict the deformation development, and the theoretical predictions were validated by the experimental data. The swelling model was applied in a finite-element analysis of a CFRD to obtain more realistic stress distributions. The analysis indicated that the wet swelling of concrete had a significant impact on the increase in tensile stress distribution in the concrete slab around the water surface.

Notation

C	diffusion concentration
C_0	surface concentration
c	width of selected layer
D	moisture diffusion coefficient
E	elastic modulus
k	bulk modulus of whole porous body
k_0	bulk modulus of solid material
M	molar weight of water
R	ideal gas constant
r	radius
S	saturation coefficient
s	capillary coefficient
T	temperature
t	time
x	position
γ	surface tension of water
ε	strain
η	dynamic viscosity
θ	contact angle
ρ	density of water
σ	capillary tensile stress

Introduction

Cracks in the facing concrete of rockfill dams often occur, especially appearing around the surface of the water on the top of the concrete faceplate in concrete-faced rockfill dams (CFRDs), as is evident in the Gongboxia and Tianshengqiao dams in China (Wang *et al.*, 2014a; Xu, 2001). Cracks, which were almost vertical, occurred in the water varying section of the Gongboxia CFRD during storage and operating periods (Chen, 2015; Wang *et al.*, 2014b). Structure- and temperature-induced stresses were considered to be the main factors causing the cracking, and the water level was described as the reason for these stresses (Chen, 2015), but uneven swelling due to water absorption has never been considered. In fact, deformations above and under the water surface due to swelling result in changes in the stress distribution and thus increase the risk of cracking. Once the formwork is removed and the surficial protection layer is damaged, concrete at the water surface layer will be exposed to the natural environment, where the relative humidity (RH) is usually much lower. This will cause the superficial concrete to become easily unsaturated. After impoundment, concrete around the surface of the water is subjected to environmental actions. The RH in the concrete under water will increase, resulting in expansion (Grasley *et al.*, 2006; Zhang *et al.*, 2011). The deformation in concrete above the water is quite different from that of the underwater concrete due to differences in the interior RH (Dimitrov *et al.*, 2007; Grasley *et al.*, 2006). Therefore, investigating this deformation phenomenon is essential to ensure dam safety.

Numerous studies on the drying shrinkage of concrete and its mechanism have been conducted. Drying shrinkage is caused by water diffusion under dry environmental conditions

(Hubler *et al.*, 2015). Previous studies have revealed the relationship between concrete shrinkage and pore moisture under constant temperature (Bažant and Yunping, 1994; Kovler, 1999; Scherer, 1990; Zhang *et al.*, 2009, 2011, 2012). Based on this relationship, several models have been proposed and used to predict the shrinkage deformation of concrete between 28 and 180 d of age (Bažant, 2001; Goel *et al.*, 2007; Kim and Lee, 1998). However, few studies on the swelling of wet concrete can be found in the literature, especially for older concrete under different levels of humidity. A few studies have shown that the swelling mechanisms of concrete vary under different environmental conditions (Goldberg *et al.*, 1975; Wittmann *et al.*, 2006). For example, for concrete above water, swelling is caused only by diffusion whereas, for concrete under water, swelling is caused by both capillary absorption and diffusion (Chin *et al.*, 1999; El-Dieb, 2007; Hall, 1989; Hanžič *et al.*, 2010; Li *et al.*, 2009; Qiu *et al.*, 2003). Obviously, swelling cannot be considered as simply the inverse process of shrinkage. It is thus very important to investigate the swelling deformation of older concrete under different environmental conditions in order to obtain realistic stress–strain distributions for finite-element (FE) analyses of concrete dams.

In the work reported in this paper, the swelling deformation of 3 year old concrete around a water surface was monitored to obtain the development curves of concrete expansion. A new theoretical swelling model was then developed to predict concrete deformation over time around a water surface. FE analysis of a typical CFRD under water pressure and considering swelling was then conducted and the realistic stress distribution obtained was analysed.

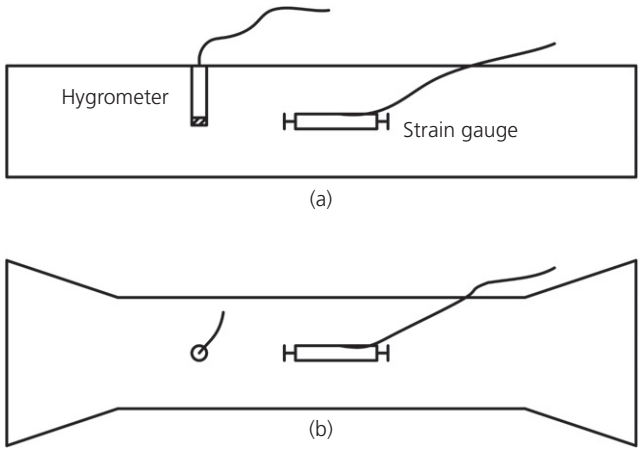

Figure 1. Positions of measuring instruments: (a) side view; (b) plan view

Research significance

Wet swelling of concrete is neglected in FE analyses of concrete faceplates near the water level in CFRDs, leading to big discrepancies in cracking patterns between simulations and on-site observations. Revealing the cracking mechanism considering swelling deformation in concrete could provide a technical basis for reducing cracks in faceplates, thus making CFRDs safer and more durable.

Experiment

Materials and specimens

The shape of the concrete specimens used in the study is shown in Figure 1. The specimens were 550 mm long and the cross-section of the intermediate portion was 100 mm × 100 mm. The mix proportions of the concrete are listed in Table 1. The 28 d and 90 d compressive strengths of cubic concrete specimens were tested and found to be 40·0 MPa and 53·1 MPa, respectively. After undergoing 28 d of curing in a standard curing room (temperature of 20°C and RH of 98%), the specimens were stored outdoors in natural environmental conditions for 3 years.

Test devices and procedures

Embedded hygrometers were used to measure the RH in the concrete specimens. The deformation and temperature of the central zone of each specimen were measured by embedded strain gauges and thermocouples. The strain gauges were 10 cm long, with measurement ranges for tensile strain and compressive strain of 0 to 1000 με and −1500 to 0 με, respectively. The indicated error was ±1 με. The measurement range of the thermocouples was −20 to 80°C, with an indicated error of ±0·1°C.

The strain gauges and hygrometers were embedded into the specimens when the concrete was poured into the moulds. The hygrometers were kept a certain distance from the strain gauges to avoid their influence on the strain gauges. The locations of the measuring instruments embedded in the concrete specimens are shown in Figure 1.

The concrete specimens were tested under the three environmental conditions listed in Table 2. Data collection was started

Table 1. Mix proportions of concrete

Constituent: kg/m^3						
Water	Cement	Fly ash	Silica fume	Sand	Gravel	Superplasticiser
154	304	140	23	767	1126	2·94

Table 2. Experimental environmental conditions

Group	Environmental conditions
A	Sealed. Specimens wrapped in impermeable membranes
B	Above water. Specimens in a sealed bucket with some water below. Bottoms of the specimens were just above the water surface. The measured RH was 90%
C	Under water. Specimens immersed in water with the water level kept just above the surfaces of the specimens

as soon as the specimens were placed in their corresponding environmental conditions. Testing was carried out in a controlled room at a temperature of 20±1°C and a RH of 35±5%.

Results

The initial RHs of the outdoor-stored specimens are shown in Table 3. Due to the local dry climate, the RHs of the specimens were low, with values in the range 55%–59%. Figure 2 shows that the temperatures in all the specimens were similar and varied within ±1°C. The interior RHs and deformations of the specimens are shown in Figure 3.

The deformation of group A remained at approximately −3 με, revealing that the autogenous deformation of 3 year old concrete was very small. This therefore indicates that the deformations of concretes in groups B and C were mainly due to changes in internal moisture.

Table 3. Initial RHs of the specimens

	Specimen number					
	1	2	3	4	5	6
Initial RH: %	55·4	58·5	59·0	58·0	56·1	56·4

As can be seen in Figure 3(a), the interior RHs of groups B and C increased with time, with the RH of group C higher than that of group B and increasing more rapidly after 10 d. Additionally, it can be observed from Figure 3(a) that the RH of group B increased approximately linearly while the RH of group C increased non-linearly.

The deformations of groups B and C also increased with time, reaching values of 27 με and 48 με at 25 d, respectively (Figure 3(b)). The global deformation–time curves obtained are logarithmic and the deformation of group C was greater than that of group B on the same test day. At the age of 7 d, the deformations of both groups B and C reached approximately 70–80% of the maximum values. In addition, during the first 7 d, the deformation of group C increased more rapidly than the deformation of group B and the total deformation of group C was twice that of group B.

The total swelling deformation of the specimens in the two groups reached values close to 30 με and 50 με, respectively, while the ultimate tensile strain of concrete is around 100 με (Swaddiwudhipong *et al.*, 2003). The swelling deformation of concrete thus accounts for 30–50% of the ultimate tensile strain. Although not large enough to cause concrete cracking, these values are relatively significant. Swelling deformation is often neglected in the literature, leading to discrepancies in concrete cracking patterns, cracking time and cracking extent between simulations and on-site observations.

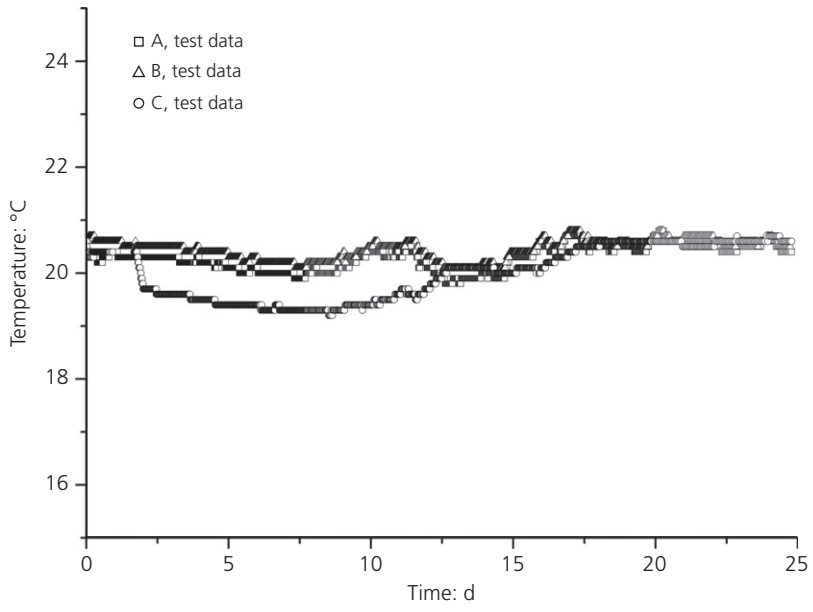

Figure 2. Development of internal temperature with time

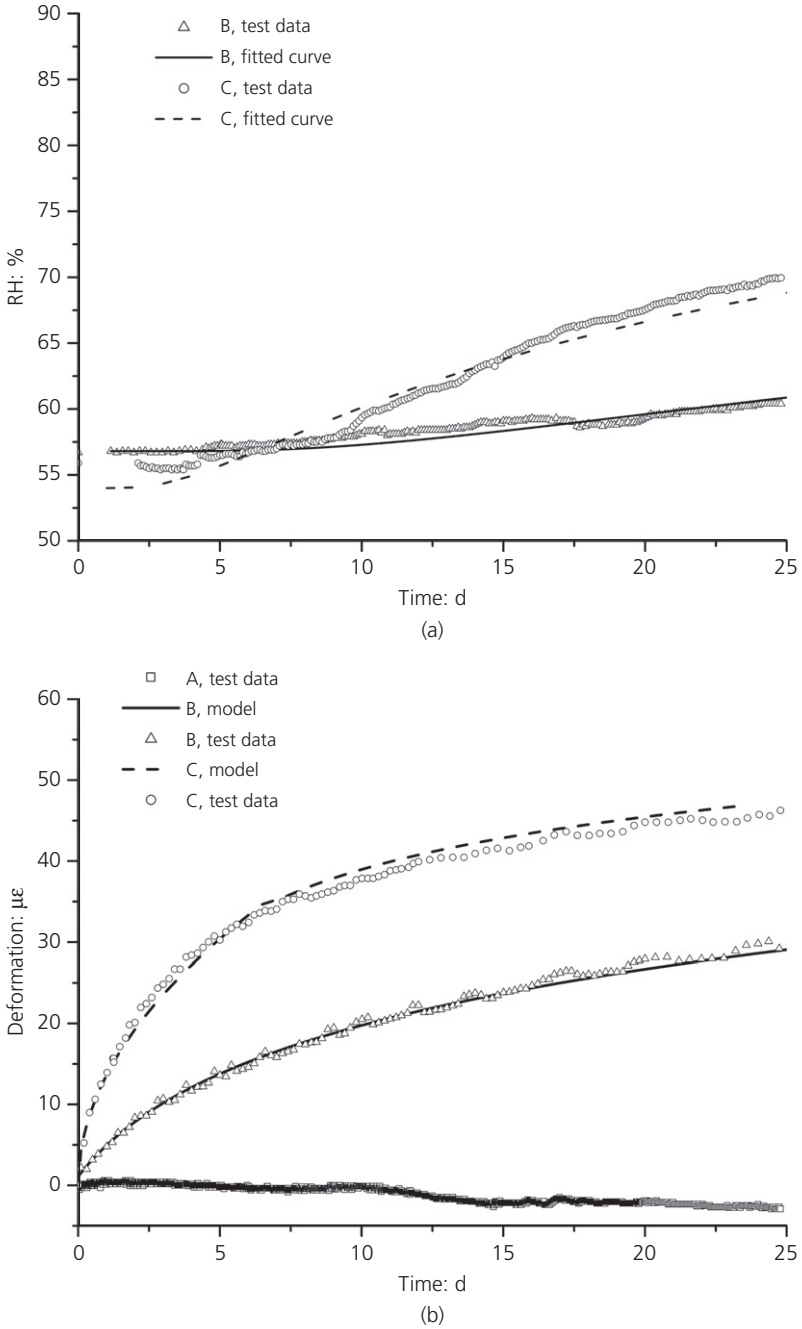

Figure 3. Temporal development of (a) interior RH and (b) deformation of specimens at the central point under different environments (positive strain represents expansion)

Theoretical modelling

The mechanism of the deformation in concrete around a water surface may be analysed as follows. The concrete pores were unsaturated before the experiment. Menisci were formed in the pores, especially in the capillary pores, which are the source of capillary tensile stress (Jensen and Hansen, 2001). The specimens shrank under the action of tensile stress in the capillaries. Water moved from the exterior to the interior, leading to a rise in the interior RH when the specimens were placed near water (or in humid environmental conditions) (Dias, 2004; Hall, 1989; Li *et al.*, 2009; Qiu *et al.*, 2003). The capillary tensile stress decreased as the RH rose, leading to expansion of the concrete. Based on this mechanism, a theoretical deformation model was developed to explain the RH and deformation changes shown in Figure 3.

Theoretical analysis of the deformation of concrete stored above water

Diffusion is the main means of water movement when concrete is located above water. This can be described by Fick's second law (Liu *et al*., 2011), expressed as

$$1. \quad \frac{\partial \mathrm{RH}}{\partial t} = \frac{\partial}{\partial x}\left(D\frac{\partial \mathrm{RH}}{\partial x}\right)$$

According to Kelvin's law, the relationship between the radius of the meniscus (r) and the interior RH is given by.

$$2. \quad r = -\frac{2\gamma M}{\ln(\mathrm{RH})\rho RT}$$

To calculate the capillary tensile stress, the Laplace equation is used. This is given by

$$3. \quad \sigma_{\mathrm{RH}} = -\frac{\ln(\mathrm{RH})\rho RT}{M}$$

Mackenzie (1950) and Bentz *et al*. (1998) assumed that capillary pores are in close proximity to cylindrical pores. The strain can then be expressed as

$$4. \quad \varepsilon = -S\left(\frac{1}{3k} - \frac{1}{3k_0}\right)\frac{\rho RT}{M}\ln(\mathrm{RH})$$

Figure 3(b) indicates that the change in the pore humidity of group B was small, so the saturation coefficient (S) is roughly constant. Meanwhile, the temperature (T) remained the same. Thus, Equation 4 can be expressed as

$$5. \quad \varepsilon = A\ln(\mathrm{RH})$$

where A is a constant coefficient. With a correlation coefficient of 0·938, Figure 4 shows that Equation 5 is appropriate to describe the relationship between deformation and RH.

To establish the relationship between deformation and time, the relationship between RH and time is needed. Martın-Pérez *et al*. (2001) suggested that the relationship between the diffusion concentration $C(x, t)$ and time could be simplified as

$$6. \quad C(x,t) = C_0\left[1 - m \times \mathrm{erf}\left(\frac{x}{2\sqrt{Dt}}\right)\right]$$

in which C_0 is the surface concentration and m is a constant coefficient. In this study, x can be regarded as constant, so the RH can be expressed as

$$7. \quad \mathrm{RH} = C_0 - a \times \mathrm{erf}\left(\frac{b}{\sqrt{t}}\right)$$

where both a and b are constant coefficients. Figure 3(a) shows that the equation agrees with the data. Thus, the theoretical deformation development with time can be expressed as

$$8. \quad \varepsilon = A\ln\left[C_0 - a \times \mathrm{erf}\left(\frac{b}{\sqrt{t}}\right)\right]$$

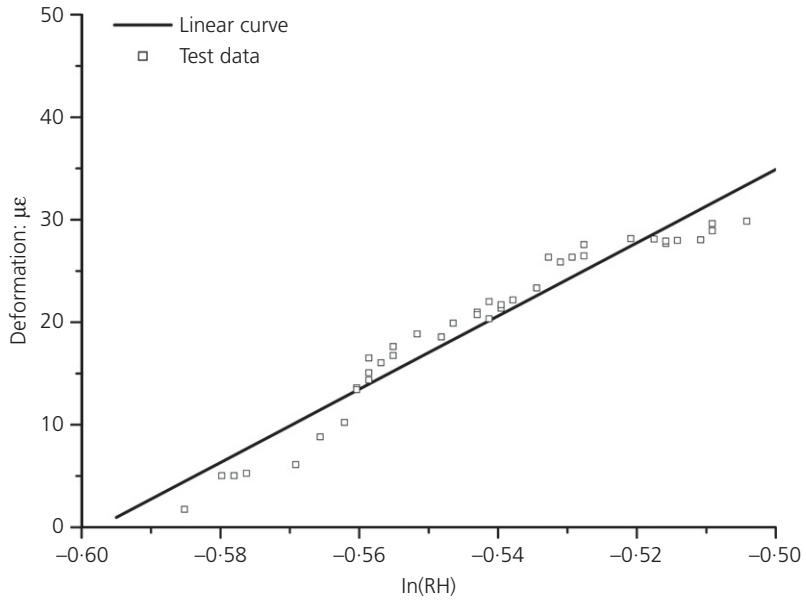

Figure 4. Relationship between deformation and RH of concrete in above-water environment and the fitting curve (with a linear correlation coefficient of 0·938)

Figure 3(b) shows that the fitting curve fits the experimental data very well, with a correlation coefficient of approximately 0·995. The deformation of concrete situated above water can thus be accurately calculated using Equation 8.

Theoretical analysis of the deformation in concrete under water

Water pressure can be neglected when concrete is located in shallow water. Water movement in this situation includes capillary absorption on the surface layer and diffusion in the interior pores. Thus, concrete under water can be divided into two regions – the saturated region and the unsaturated region. The boundary of the two regions is the water absorption front, and diffusion only exists in the unsaturated region. Both types of water movement can cause an increase in deformation and the theoretical analyses are as follows.

During the absorption process, the water-saturated region expands and the absorption front moves inwards. The humidity in the pores is approximately RH_0 before the arrival of the front, and becomes 100% soon after the arrival. According to Equation 3, the stress change in this process is

$$9.\quad \Delta\sigma = \sigma_{100\%} - \sigma_0 = -\sigma_0 = \frac{\rho RT}{M}\ln(RH_0)$$

A thin unit-length layer in the centre of the specimen was chosen to analyse the deformation caused by the changes in stress. The stress condition of this layer is shown in Figure 5(a). Each side of the layer is subjected to a body force of $\Delta\sigma$. As shown in Figure 5(b), by breaking the layer into saturated and unsaturated regions, the interfaces of the two regions would be subjected to a surface force of $x\Delta\sigma$, where x is the absorption depth. Thus, the central deformation of the specimen can be calculated by analysing the stress condition shown in Figure 5(c).

The width of the selected layer is assumed to be c (m) and the width of the unsaturated region is $c-2x$. Thus, the central deformation of the specimen can be calculated as

$$10.\quad \varepsilon = \frac{2\Delta\sigma x}{(c-2x)E}$$

The ultimate absorption depth due to capillary suction is approximately 10 mm in ordinary concrete with an air-entraining agent when the temperature is approximately 20°C (Hanžič *et al.*, 2010). This depth is only a few millimetres, which is much smaller than c, especially at an early absorption time. Thus, the following approximation can be made

$$11.\quad \varepsilon = \frac{2\Delta\sigma x}{(c-2x)E} = \frac{\Delta\sigma(-c+2x+c)}{(c-2x)E} = -\frac{\Delta\sigma}{E} + \frac{\Delta\sigma}{E[1-(2x/c)]} \approx \frac{2\Delta\sigma x}{cE}$$

In addition, the relationship between the central deformation and the absorption depth can be expressed as

$$12.\quad \varepsilon = \frac{2\rho RT}{cEM}\ln(RH_0)x$$

The development of absorption depth with time can be calculated using the Newton dynamic equation. The Lucas–Washburn equation (Lucas, 1918; Washburn, 1921) is the solution, which is expressed as

$$13.\quad x = s\sqrt{t}$$

In Equation 13, the capillary coefficient (s) is defined as

$$14.\quad s = \sqrt{\frac{\gamma r\cos\theta}{2\eta}}$$

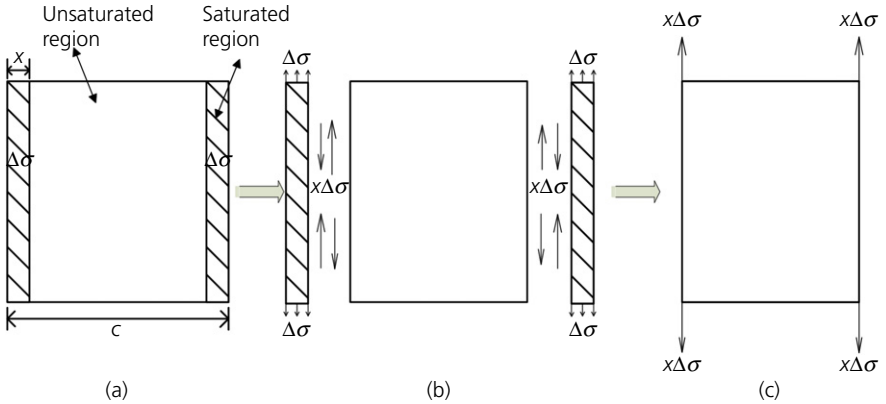

Figure 5. Force model of the selected layer

Thus, the relationship between time and central deformation can be expressed as

$$\varepsilon = \frac{2\rho RT}{cEM}\ln(\mathrm{RH}_0)\sqrt{\frac{\gamma r\cos\theta}{2\eta}}\sqrt{t} \quad (15)$$

where all of the parameters except t can be replaced by a constant K_1, considering that all the other parameters are constant or nearly invariant. Thus, Equation 15 can be written simply as

$$\varepsilon_1 = K_1\sqrt{t} \quad (16)$$

Equation 16 indicates that there is a linear relationship between the central deformation and the square root of time during the water absorption process.

During the diffusion process, water migrates in the concrete pores of the unsaturated region. The relationship between the central deformation and the pore RH can be described by Equation 5, and the relationship between RH and time can be described by Equation 7. Thus, the central deformation due to the diffusion process is

$$\varepsilon_2 = A'\ln\left[C_0' - a'\times\mathrm{erf}\left(\frac{b'}{\sqrt{t}}\right)\right] \quad (17)$$

where A', a' and b' are constant coefficients.

The concrete pores in the surface layer have a strong water-absorbing capacity in the early stage. Therefore, compared with the diffusion process, absorption dominates the development of deformation. The increase in absorption depth slows the longer concrete is exposed to water, and eventually stops (Hanžič *et al.*, 2010). Then, the diffusion process takes over, dominating the process of deformation. Equation 16 can thus be used to predict deformation at the early stage and Equation 17 can be used at the later stage. Thus, the theoretical deformation model of concrete submerged in water can be expressed as

$$\varepsilon = \begin{cases} K_1\sqrt{t} & t \le t_0 \\ A'\ln\left[C_0' - a'\times\mathrm{erf}\left(\frac{b'}{\sqrt{t}}\right)\right] + K_1\sqrt{t_0} & t \ge t_0 \end{cases} \quad (18)$$

where t_0 is the time that distinguishes the early stage from the late stage. To obtain t_0, the global relationship between deformation and ln(RH) was plotted. As shown in Figure 6, there is an obvious turning point in the curve, after which an obvious linear relationship exists. Another relationship exists before the turning point, which is shown in Figure 7, where $\varepsilon = K_1\sqrt{t}$. Thus, the turning point represents t_0, which can be determined from Equation 18 as 7·2 d.

Comparisons of the model predictions and the experimental data are shown in Figure 3(b). The underwater specimens (group C) showed very good agreement between the prediction and the test data, with a correlation coefficient of 0·9881.

Therefore, the theoretical swelling model of aged concrete around a water surface can be expressed as follows. For concrete above water

$$\varepsilon = A\ln\left[C_0 - a\times\mathrm{erf}\left(\frac{b}{\sqrt{t}}\right)\right] \quad (19a)$$

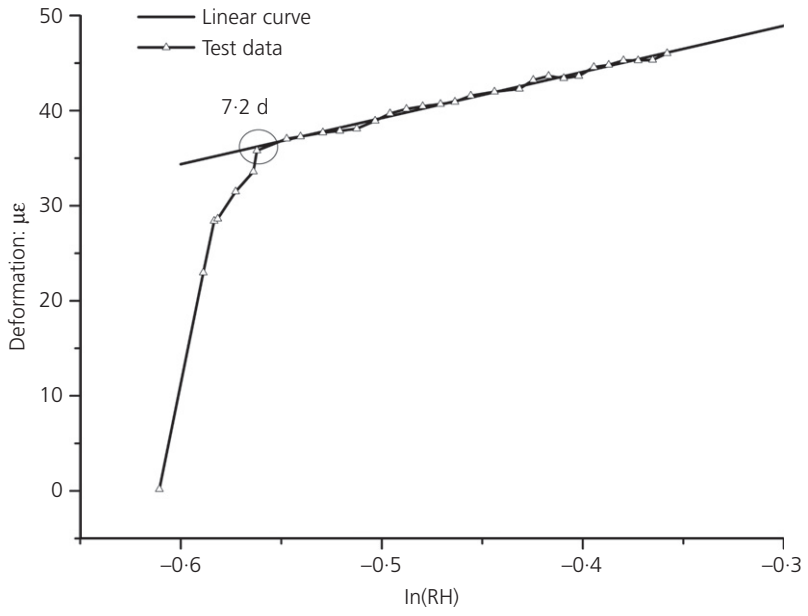

Figure 6. Deformation against the natural logarithm of RH for underwater specimens

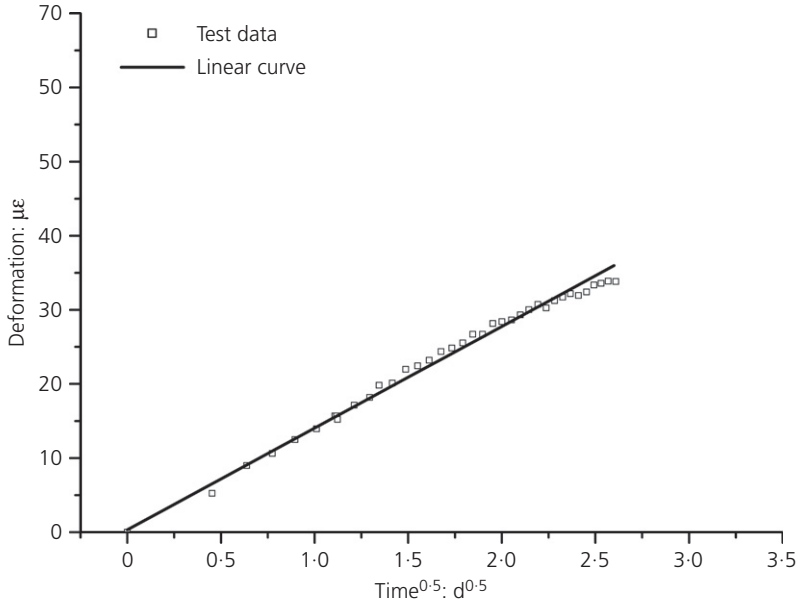

Figure 7. Deformation plotted against square root of time for underwater specimens (linear correlation coefficient is 0·989)

and for concrete under water

$$\varepsilon = \begin{cases} K_1\sqrt{t} & t \le t_0 \\ A' \ln\left[C_0' - a' \times \operatorname{erf}\left(\dfrac{b'}{\sqrt{t}}\right)\right] + K_1\sqrt{t_0} & t \ge t_0 \end{cases} \quad \text{19b.}$$

Discussion of the swelling of concrete around a water surface

The deformation formulae were deduced by establishing the relationship between deformation and RH in the pores using the Laplace equation. Diffusion is the only type of water migration in concrete above water, so swelling in this case can be regarded as the inverse process of shrinkage in an above-water environment. However, the prediction is not suitable for underwater concrete because the swelling in this case is caused by both water diffusion and capillary absorption. A theoretical equation to predict the expansion of concrete under water was achieved by introducing the Lucas–Washburn equation into the analysis. The upper limit of RH is C_0, which is less than 100% in the model.

The differences in swellings of concrete in above- and below-water conditions are as follows. Because of the different environmental conditions, different types of water migration occurred in the concrete. Diffusion driven by a humidity gradient is the main type of pore water migration in an above-water environment. The low moisture migration speed and the slow increase in pore humidity lead to slow swelling deformation (Parrott, 1994; Qiu *et al.*, 2003; Šelih *et al.*, 1996). For concrete in an underwater environment, the main type of water migration is capillary absorption driven by capillary suction in the surface layer and diffusion in the pores (Wang and Ueda, 2011; Zhmud *et al.*, 2000). The capillary absorption process has two features: (*a*) the pores will be immediately filled with water in the absorption region; (*b*) the absorbing rate is higher initially. Swelling thus increases rapidly as a result of the two types of water migration.

The difference in deformation between the two conditions shows that the maximum deformation difference occurred on day 7, as shown in Figure 8. This difference is the cause of

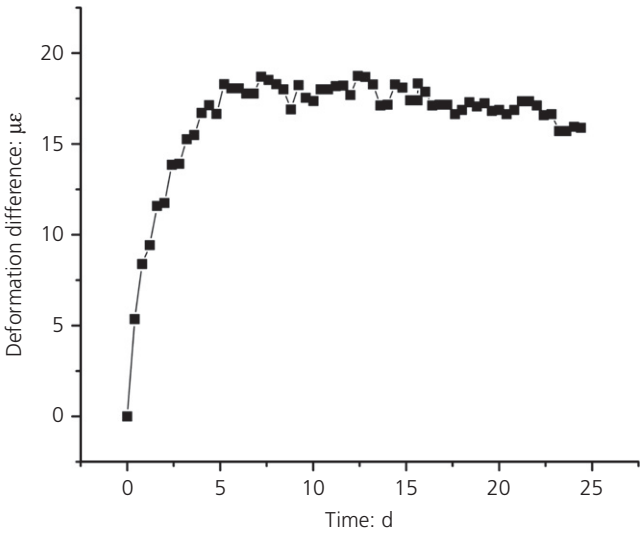

Figure 8. Difference in deformation for specimens under water and above water

tensile stress in concrete around the water surface, which is analysed in the following.

Finite-element analysis of CFRDs

After impoundment, a portion of the concrete faceplate in a CFRD would be near the surface of the water, and thus swelling deformation has to be considered in the FE analysis. The swelling model was embedded in an FE stress analysis of the Gongboxia CFRD. Stress analysis of the CFRD around the surface of the water, considering swelling, is analysed and discussed in this section.

Finite-element model

The FE model of the Gongboxia CFRD, which includes eight concrete faceplates of thickness 0·5 m, is shown in Figure 9. Because the focus in this study was the area around the top of the central concrete slab, other parts of the dam were ignored to simplify the calculation. The maximum height of the dam is 132 m and the crest length is 128 m. A total of 16 000 octahedral isoparametric elements were used in the analysis.

Initial conditions

The initial air temperature was set as −10°C, based on the actual average temperature in winter. The initial RH was set as 50%, in accordance with the initial conditions of the 3 year old concrete (Table 3). The initial stress condition was simply the result of gravity.

Material properties and boundary conditions

The material properties of the CFRD are listed in Table 4. The tensile cracking stress was set at 2 MPa (Zhu *et al.*, 2013). Water pressure, gravity, water temperature, air temperature and swelling were the main boundary conditions taken into account in the analysis. The water level was 128 m and the water temperature was 15°C. The displacements of the bottom nodes were fixed and the temperature of the downstream face was set to the air temperature.

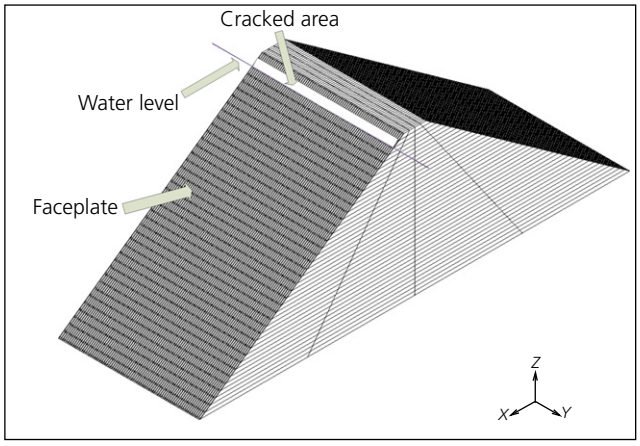

Figure 9. Finite-element model of the CFRD

Table 4. Material properties of the CFRD

	Concrete	Rockfill
Thermal diffusivity: m^2/d	0·0903	0·0694
Density: kg/m^3	2395	2080
Elastic modulus: MPa	25 000	235
Poisson's ratio	0·167	0·3
Linear expansion coefficient: $\times 10^{-6}$/°C	10·05	0·85

Numerical modelling

The thermal–mechanical elements in the non-linear FE analysis solution Marc (MSC, 2000) were used in the FE analysis, and the wet expansion was calculated by modifying the creep module. The stress was then calculated by multiplying the elastic modulus by the overall deformation, which was obtained by summing the thermal expansion and the wet expansion.

Calculated conditions

A numerical example according to the actual boundary conditions was first used for the analysis. Eight different cases with air temperatures ranging from −20°C to 15°C were then analysed. In each case, the tensile stresses with and without consideration of wet expansion were compared to determine the proportion of the tensile stress due to wet expansion.

Results and discussion

As mentioned earlier in the paper, many cracks were observed in the concrete faceplate of Gongboxia CFRD around the surface of the water after an increase in water level. This phenomenon is likely caused by the effects of the discordance of temperature and moisture distribution.

In the modelling, the air temperature was first set to −10°C, which is the in situ air temperature of Gongboxia dam. The maximum tension stress occurred on day 8, which is close to the time of the maximum swelling difference in the concrete around the water surface. A tensile region was found around the surface of the water with a maximum tensile stress of more than 2 MPa, indicating a high cracking risk (Figure 10(a)). Because water pressure and gravity make no contribution to the tensile stress, the tensile stress was primarily caused by the differences in temperature and moisture conditions above and below the water. For example, concrete above the water would shrink more than the concrete under water, causing tensile stress around the water level if the air temperature is lower than the water temperature. In addition, swelling of the concrete under water would be greater than that of the concrete above the water.

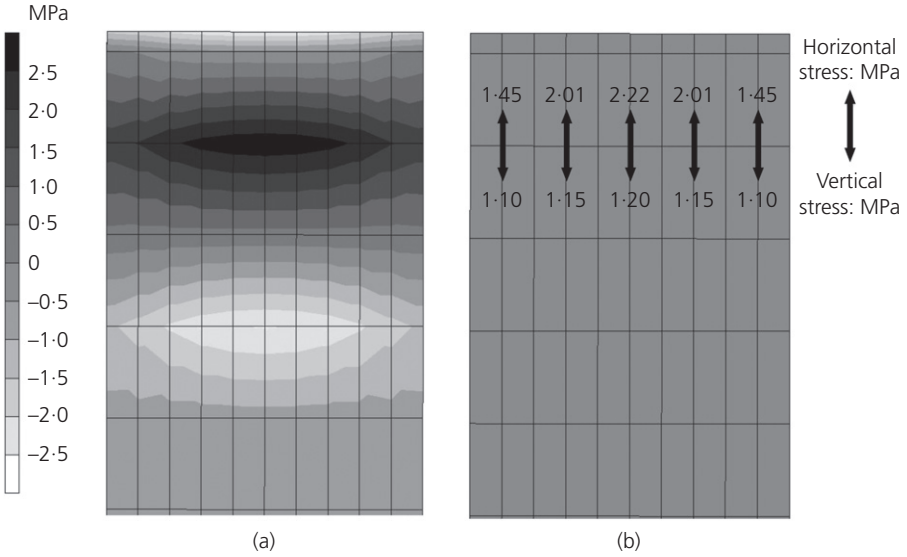

Figure 10. Calculated (a) stress distributions and (b) stress decomposition

The stress was decomposed into horizontal and vertical stresses to determine the cracking direction. As shown in Figure 10(b), the face slab suffered more horizontal stress than vertical stress. The maximum stress was 2·22 MPa, in the middle of the slab near the water level, so cracking is more likely to be in the vertical direction. As already mentioned, actual cracks in Gongboxia dam were observed in the section of water level variability and these cracks were mostly vertical (Chen, 2015). The modelling results thus appropriately explain the causes of the actual cracks in Gongboxia dam; that is, the changing water level was the main cause of cracking in the face slab of the dam. In addition, several horizontal cracks were found in the faceplate of the dam, which are likely caused by a short period of rapid cooling or insulation failure. However, no horizontal cracking was found in the modelling because these factors were not considered in the simulation.

A series of cases with eight different air temperatures was considered to determine the percentage of the tensile stress due to swelling. The percentage of the tensile stress caused by wet swelling is shown in Figure 11. The figure shows that the higher the air temperature, the greater the contribution of wet swelling to tensile stress, and vice versa. The temperature of the water thus contributes to the amount of wet swelling and should be considered.

In summary, the wet swelling of concrete has obvious impacts on the stress distribution in concrete around a water surface. More realistic stress distributions could thus be obtained by considering swelling in FE analyses of CFRDs.

Conclusion

The development of swelling in concrete located under and above water was analysed. Concrete swelling can be regarded

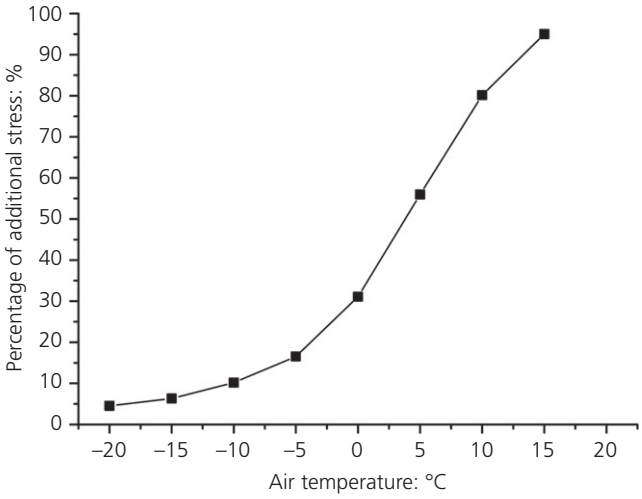

Figure 11. Percentage of additional tensile stress caused by wet swelling at different air temperatures

as the inverse process of drying shrinkage in above-water conditions because diffusion is the only type of water migration that leads to an increase in internal RH and deformation. However, for concrete under water, absorption dominates the development of deformation at the early stage and diffusion dominates the swelling at the late stage. These differences result in different deformations in concrete around the surface of water in the first several days of contact.

A theoretical model to predict the swelling deformation of concrete around a water surface was developed. The model is based on Fick's second law, the Laplace equation, the Lucas–Washburn equation and the material mechanics method, where moisture movement and the development of stress in the

capillary pores are the main mechanisms. The model simply and accurately describes concrete swelling both above and below water. Good agreement between the experimental results and the model predictions was obtained.

In addition, FE analysis of a concrete-faced rockfill dam (CFRD) considering wet swelling of concrete indicated that wet swelling of the concrete would cause a significant increase in tensile stress and the risk of cracking in the concrete slab in the section where the water level is variable, especially when the weather is not too cold. More realistic and reliable stress distributions can be obtained in FE analyses of CFRDs if wet swelling is considered.

Acknowledgements

This work was supported by the National Nature Science Key Foundation of China (51279087 and 51339003), a Research Project of the State Key Laboratory of Hydroscience and Engineering of Tsinghua University (2015-C-02) and a Research Project of the State Key Laboratory of Simulation and Regulation of Water Cycles in River Basins (IWHR-SKL-21412).

REFERENCES

Bažant ZP (2001) Prediction of concrete creep and shrinkage: past, present and future. *Nuclear Engineering and Design* **203(1)**: 27–38.

Bažant ZP and Yunping X (1994) Drying creep of concrete: constitutive model and new experiments separating its mechanisms. *Materials and Structures* **27(1)**: 3–14.

Bentz DP, Garboczi EJ and Quenard DA (1998) Modelling drying shrinkage in reconstructed porous materials: application to porous Vycor glass. *Modelling and Simulation in Materials Science and Engineering* **6(3)**: 211.

Chen N (2015) Analysis on causes of cracks in concrete face slabs in water variation section of Gongboxia concrete face rockfill dam. *Northwest Hydropower* **2015(6)**: 23–27.

Chin JW, Nguyen T and Aouadi K (1999) Sorption and diffusion of water, salt water, and concrete pore solution in composite matrices. *Journal of Applied Polymer Science* **71(3)**: 483–492.

Dias W (2004) Influence of drying on concrete sorptivity. *Magazine of Concrete Research* **56(9)**: 537–543, http://dx.doi.org/10.1680/macr.2004.56.9.537.

Dimitrov D, Milchev A and Binder K (2007) Capillary rise in nanopores: molecular dynamics evidence for the Lucas-Washburn equation. *Physical Review Letters* **99(5)**: 054501.

El-Dieb A (2007) Self-curing concrete: water retention, hydration and moisture transport. *Construction and Building Materials* **21(6)**: 1282–1287.

Goel R, Kumar R and Paul D (2007) Comparative study of various creep and shrinkage prediction models for concrete. *Journal of Materials in Civil Engineering* **19(3)**: 249–260.

Goldberg J, O'Toole K and Roper H (1975) Holographic interferometry for measuring swelling of hardened concrete. *ASTM Journal of Testing and Evaluation* **3(4)**: 263–270.

Grasley ZC, Lange DA and Matthew D (2006) Internal relative humidity and drying stress gradients in concrete. *Materials and Structures* **39(9)**: 901–909.

Hall C (1989) Water sorptivity of mortars and concretes: a review. *Magazine of Concrete Research* **41(147)**: 51–61, http://dx.doi.org/10.1680/macr.1989.41.147.51.

Hanžič L, Kosec L and Anžel I (2010) Capillary absorption in concrete and the Lucas–Washburn equation. *Cement & Concrete Composites* **32(1)**: 84–91.

Hubler MH, Wendner R and Bažant ZP (2015) Statistical justification of model B4 for drying and autogenous shrinkage of concrete and comparisons to other models. *Materials and Structures* **48(4)**: 797–814.

Jensen OM and Hansen PF (2001) Autogenous deformation and RH-change in perspective. *Cement and Concrete Research* **31(12)**: 1859–1865.

Kim JK and Lee CS (1998) Prediction of differential drying shrinkage in concrete. *Cement and Concrete Research* **28(7)**: 985–994.

Kovler K (1999) A new look at the problem of drying creep of concrete under tension. *Journal of Materials in Civil Engineering* **11(1)**: 84–87.

Li K, Li C and Chen Z (2009) Influential depth of moisture transport in concrete subject to drying–wetting cycles. *Cement & Concrete Composites* **31(10)**: 693–698.

Liu X, Chia KS and Zhang MH (2011) Water absorption, permeability, and resistance to chloride-ion penetration of lightweight aggregate concrete. *Construction and Building Materials* **25(1)**: 335–343.

Lucas R (1918) Rate of capillary ascension of liquids. *Kolloid-Zeitschrift* **23(15)**: 15–22.

Mackenzie J (1950) The elastic constants of a solid containing spherical holes. *Proceedings of the Physical Society: Section B* **63(1)**: 2.

Martın-Pérez B, Pantazopoulou S and Thomas M (2001) Numerical solution of mass transport equations in concrete structures. *Computers & Structures* **79(13)**: 1251–1264.

MSC (MSC Software Corporation) (2000) Marc. Advanced Nonlinear Simulation Solution. MSC, Newport Beach, CA, USA.

Parrott L (1994) Moisture conditioning and transport properties of concrete test specimens. *Materials and Structures* **27(8)**: 460–468.

Qiu X, Haghighat F and Kumaran MK (2003) Moisture transport across interfaces between autoclaved aerated concrete and mortar. *Journal of Thermal Envelope and Building Science* **26(3)**: 213–236.

Scherer GW (1990) Theory of drying. *Journal of the American Ceramic Society* **73(1)**: 3–14.

Šelih J, Sousa AC and Bremner TW (1996) Moisture transport in initially fully saturated concrete during drying. *Transport in Porous Media* **24(1)**: 81–106.

Swaddiwudhipong S, Lu HR and Wee TH (2003) Direct tension test and tensile strain capacity of concrete at early age. *Cement and Concrete Research* **33(12)**: 2077–2084.

Wang L and Ueda T (2011) Mesoscale modeling of water penetration into concrete by capillary absorption. *Ocean Engineering* **38(4)**: 519–528.

Wang ZJ, Liu SH, Li LJ and Wang LJ (2014a) Numerical analysis of the causes of slab's cracks on Gongboxia face rockfill dam. *Journal of Hydraulic Engineering* **45(3)**: 343–350.

Wang Z, Liu S, Vallejo L and Wang L (2014b) Numerical analysis of the causes of face slab cracks in Gongboxia rockfill dam. *Engineering Geology* **181**: 224–232, https://doi.org/10.1016/j.enggeo.2014.07.019.

Washburn EW (1921) The dynamics of capillary flow. *Physical Review* **17(3)**: 273.

Wittmann F, Beltzung F and Meier S (2006) Shrinkage and swelling of concrete without capillary condensed water. *Restoration of Buildings and Monuments* **12(1)**: 35–42.

Xu M (2001) Reason analysis of the crack in the faceplate of the Tianshengqiao I rockfill dam. *Hongshui River* **20(3)**: 40–41.

Zhang J, Qi K and Huang Y (2009) Calculation of moisture distribution in early-age concrete. *Journal of Engineering Mechanics* **135(8)**: 871–880.

Zhang J, Gao Y and Han Y (2011) Interior humidity of concrete under dry-wet cycles. *Journal of Materials in Civil Engineering* **24(3)**: 289–298.

Zhang J, Hou D and Han Y (2012) Micromechanical modeling on autogenous and drying shrinkages of concrete. *Construction and Building Materials* **29(3)**: 230–240.

Zhmud B, Tiberg F and Hallstensson K (2000) Dynamics of capillary rise. *Journal of Colloid and Interface Science* **228(2)**: 263–269.

Zhu J, Wang Y and Zhang M (2013) Mechanism analysis of vertical cracks on face slab of Gongboxia CFRD. *Water Power* **39(4)**: 40–42.